Chemical Science

ROYAL SOCIETY OF CHEMISTRY

EDGE ARTICLE

View Article Online
View Journal | View Issue

Cite this: *Chem. Sci.*, 2025, **16**, 6231

All publication charges for this article have been paid for by the Royal Society of Chemistry

Continuous porous aromatic framework membranes with acid-/base-induced reversible isomerization for switchable ion conductivity†

Jian Song,‡ Hengtao Lei,‡ Lin Lin, Mengxiao Sun, Xueyan Han, Zilong Dou, Yuyang Tian * and Guangshan Zhu *

Received 11th December 2024
Accepted 1st March 2025

DOI: 10.1039/d4sc08389j

rsc.li/chemical-science

Stimuli-responsive ion conductor materials are highly sought after in the fields of biological systems, clean energy, and smart devices. However, it remains a huge challenge to achieve acid/base switchable ion conductors owing to their stringent requirements of structural responsive behaviors, high stability and porosity. In this study, porous aromatic frameworks (PAFs) are utilized as a favorable platform to successfully design and prepare ion conductive powders and its continuous membranes based on a commercially available pH indicator. Interestingly, these PAFs possessed structural reversibility in response to acidic and alkaline environments, followed by an apparent ion-conducting switch of about 4 orders of magnitude (from 3.36×10^{-7} S cm^{-1} to 4.59×10^{-3} S cm^{-1}) under the conditions of 25 °C and 98% RH. Moreover, the continuous PAF membrane exhibited an ultrahigh ion conductivity of 7.29×10^{-1} S cm^{-1} after 1 mol per L NaOH treatment and good acid/base switchable cycle stability. To our knowledge, this is the first report on exploring ion-conductive porous frameworks and continuous membranes that dynamically respond to acid/base chemical stimuli. This work provides a new research strategy for the application of ion conductors as so-called "smart materials" even in extremely harsh chemical environments.

Introduction

Biological systems display many responsive behaviors to external stimuli while exhibiting excellent environmental adaptability.[1,2] Stimuli-responsive materials inspired from these natural systems have continuously aroused widespread interest in numerous interdisciplinary fields during the past decades.[3–8] These "smart materials" can respond to various stimuli, including light, heat, sound waves, electric field, solvent, pH, and stress, expanding their applications to energy storage and conversion, biomedicine, sensing, imaging, and coatings.[9–18] In this context, stimuli-induced ion transport materials have attracted great attention owing to their broad application prospects in biological systems, clean energy, and smart devices.[19–23] Stimuli-responsive ion conductors can achieve the transmission and processing of electrical signals *via* ionic currents. Together with stimuli-responsiveness, open frameworks of host materials, such as MOFs and COFs, can also provide multiple functions for drug delivery, sensors, memristors, and display devices based on the stimuli, such as guest molecules, light, voltage, and electric field transistors.[24–27] Currently, many application scenarios need timely monitoring of the acidic and alkaline environments, such as the detection of acidic and alkaline tail gas emissions. In this case, the realization of ion conductor detection devices that respond to acidic and alkaline stimuli by communicating and processing electrical signals *via* ionic currents will greatly expand the application potential of ion conductors and thereby promote the further development of materials science and chemistry. Nevertheless, it undoubtedly puts forward highly stringent requirements for a dynamic structural design as well as high stability and porosity, which remain huge challenges.

Porous aromatic frameworks (PAFs) are representative porous materials with high surface area and high stability and can withstand harsh environments, such as strong acids, strong bases, high heat, and high humidity.[28–30] The structures and pore properties of PAFs can be regulated by designing their building units and modifying the frameworks, which demonstrate different performances and applications in the fields of adsorption, separation, catalysis, sensing and energy.[31–43] It is well-known that porous materials, including metal–organic frameworks (MOFs) and covalent organic frameworks (COFs), exhibit great potential in energy storage.[44–51] The open channels with good tunability ensure that they serve as an ideal platform to investigate ion-transport behaviors inside atomically precise

Key Laboratory of Polyoxometalate and Reticular Material Chemistry of Ministry of Education, Faculty of Chemistry, Northeast Normal University, Changchun, Jilin 130024, China. E-mail: tianyy100@nenu.edu.cn; zhugs@nenu.edu.cn

† Electronic supplementary information (ESI) available. See DOI: https://doi.org/10.1039/d4sc08389j

‡ These authors contributed equally to this work.

skeletons, which is of fundamental importance for achieving solid electrolytes with high ion conduction ability. Moreover, the high surface areas, rich structural tunability, and functional pore surface of porous materials provide great opportunities to load a variety of guest molecules as ion carriers and to systemically modify the ion concentration and mobility within the available spaces. Thus, the structural designability and high stability of PAFs offer new opportunities for the development of acid/base stimuli-responsive ion conductors.

Current researches on the ion conductivity of porous materials are mostly carried out using their powder form, which is difficult to be used as membranes for further application owing to their insolubility. The stacking voids of powders reduce the ion transport efficiency to some extent. Meanwhile, composite membranes based on powders and polymers also hinder the transfer of ions and are not conducive to the analysis of ion transport mechanisms due to the non-functional polymer components. Hence, there is intense demand for the design and preparation of cutting-edge continuous ion conductive membranes to extend their application in actual acid–base response monitoring devices. However, the polymerization process of most PAF materials generally requires a catalyst and an inert atmosphere, making it difficult to prepare membranes like COFs or MOFs using fabrication strategies like interfacial polymerization, solvothermal synthesis, *etc.*[52–54] Consequently, constructing continuous PAF ion conductive membranes is another important challenge in current research.

Herein, two porous aromatic frameworks (named PAF-125 and PAF-126) have been designed and synthesized by employing a commercially available acid/base indicator (bromophenol blue, BPB) as the responsive building unit (Fig. 1). As expected, these PAF materials exhibit high porosity and structural responsive behaviors to acidic and alkaline environments. At 25 °C and 98% RH, the PAF powder exhibited an interesting switch in ion conductivity from 3.36×10^{-7} S cm^{-1} after 1 mol per L HCl treatment to 4.59×10^{-3} S cm^{-1} after 1 mol per L NaOH treatment, achieving a change in value of 4 orders of magnitude for the acid/base switch. Subsequently, a continuous PAF membrane was prepared by the strategy of surface-initiated polymerization (SIP). We unexpectedly found that the continuous PAF membrane exhibited ultrahigh ion conductivity after 1 mol per L NaOH treatment, reaching up to 7.29×10^{-1} S cm^{-1} (85 °C, 98% RH), as well as good cycle stability of the acid/base switchable ion conductivity. To our knowledge, this is the first report of an ion conductive membrane that responds dynamically to chemical acid/base stimulus. This study provides a new research strategy for the exploration of intelligent ion conductive membranes in the future.

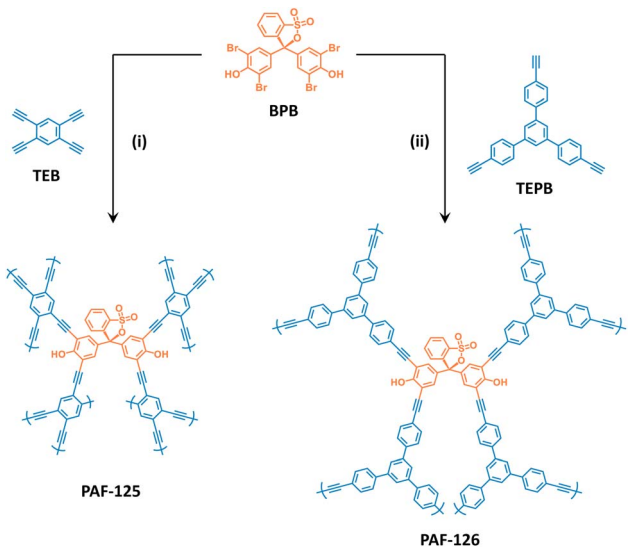

Fig. 1 Schematic of the synthesis of PAFs using bromophenol blue (BPB) (i) and (ii): $Pd(PPh_3)_4$/CuI and DMF/Et_3N, respectively, at 100 °C.

Results and discussion

Material synthesis and characterization

The successful synthesis and structural characterization of PAF materials was carried out using a series of spectroscopic methods and elemental analysis techniques. The Fourier-transform infrared (FTIR) spectra of PAFs are shown in Fig. 2a. The characteristic peaks found at 535 cm^{-1} in the BPB spectrum disappeared in the PAFs spectra, indicating that the phenyl-Br groups of the monomer BPB had almost completely coupled with the alkyne group. Furthermore, a new vibration peak appeared at 2200 cm^{-1} in the spectrum of PAFs, which could be attributed to the C≡C stretching vibration of the RC≡CR group, indicating the occurrence of polymerization. For PAF-125, an additional C≡C stretching vibration at 2100 cm^{-1} and unsaturated ≡CH bending vibration at 3280 cm^{-1} originating from the unreacted alkynyl groups (RC≡CH) were observed. This may be because steric hindrance prevents complete polymerization owing to the closely located alkyne active sites of the TEB monomers. In addition, a typical S=O stretching vibration was observed at 1190 cm^{-1} and 1230 cm^{-1}, indicating the presence of sultone groups in PAFs.[55,56] More detailed IR spectra of PAFs, BPB, and aromatic acetylene monomers are provided in Fig. S1 and S2.†

To study the porosities of the PAF materials, the N_2 adsorption isotherms of activated samples were measured at 77 K. As shown in Fig. 2b, PAF-125 exhibited characteristics of microporous adsorption at low relative pressure, while an obvious hysteresis loop was observed at medium relative pressure from 0.4 to 0.6 p/p_0, indicating the presence of additional mesoporous structure. The observed Brunauer–Emmett–Teller (BET) surface area and pore volume were 87.9 m^2 g^{-1} and 0.075 cm^3 g^{-1}, respectively. According to nonlocal density functional theory (NLDFT) calculations, PAF-125 has four kinds of pore sizes with diameters of 0.54 nm, 1.01 nm, 1.39 nm and 3.95 nm, respectively (Fig. S3†). The N_2 adsorption isotherm of PAF-126 material was a typical type I adsorption curve, indicating that the material has a microporous network structure. The BET surface area was 597.9 m^2 g^{-1} with a pore volume of 0.311 cm^3 g^{-1}. The pore size distribution of PAF-126 was mainly concentrated in the micropore range of less than 2 nm, presenting two kinds of pore sizes (0.54 nm and 1.06 nm, respectively) (Fig. S4†). Moreover, the water affinity of the pore structure is

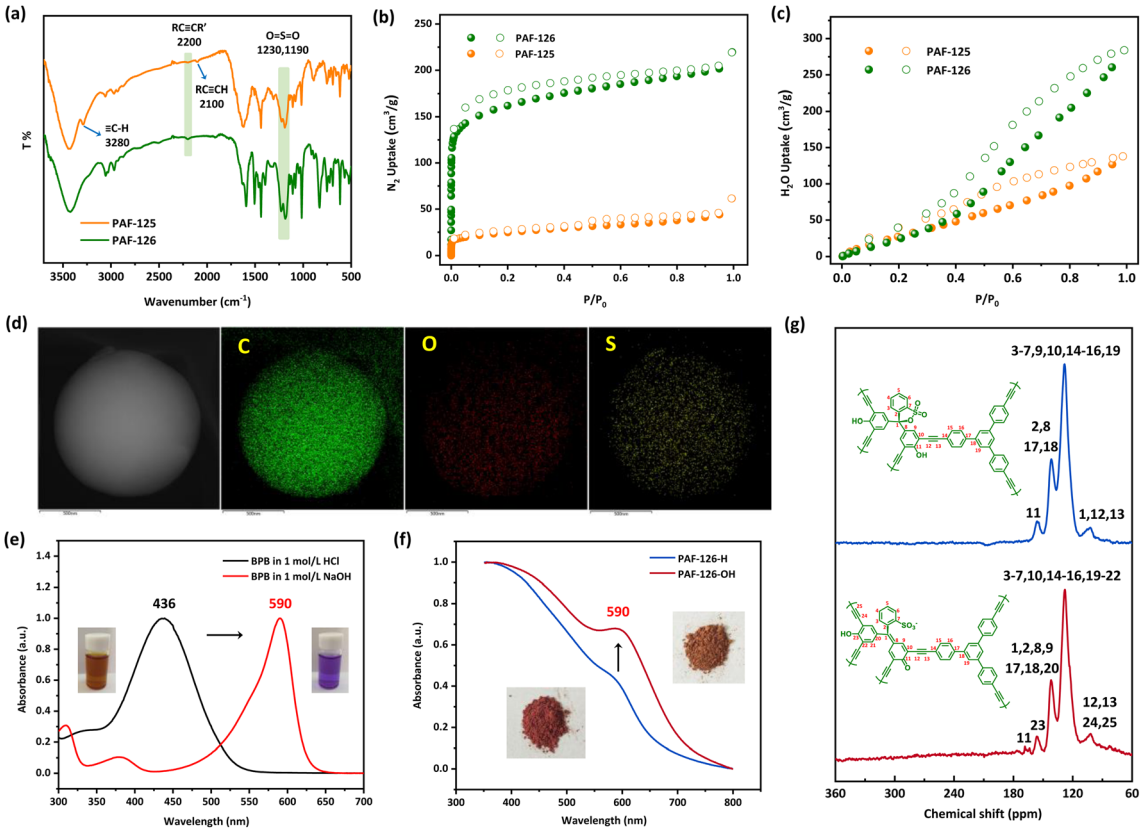

Fig. 2 (a) FTIR spectra of PAFs. (b) N_2 adsorption–desorption isotherms of PAFs measured at 77 K (adsorption branch is labeled with filled symbols). (c) H_2O adsorption–desorption isotherms of PAFs measured at 298 K (adsorption branch is labeled with filled symbols). (d) EDS elemental mapping images of PAF-126. (e) UV-vis spectra and color contrast images of bromophenol blue in 1 mol per L HCl and 1 mol per L NaOH solutions. (f) UV-vis spectra and color contrast images of PAF-126 after treatment with 1 mol per L HCl and 1 mol per L NaOH. (g) ^{13}C solid-state NMR spectra of PAF-126-H and PAF-126-OH.

also important to the ion conductivity performance of porous materials.

Therefore, the water vapor adsorption isotherms of PAF materials were obtained at 298 K. Both PAF-125 and PAF-126 exhibited good water vapor adsorption capacity at low relative pressures, and it gradually increased, reaching 138 $cm^3\ g^{-1}$ and 284 $cm^3\ g^{-1}$ at 0.96 p/p_0, respectively, as shown in Fig. 2c. The results show that the pores of the two materials have good affinity for water, which is conducive to the adsorption and transfer of water molecules inside the framework and will further promote the ion conductive efficiency. Moreover, the X-ray diffraction patterns (Fig. S5 and S6†) indicated that the PAFs were amorphous in nature, which is beneficial to isotropic ion transport.[42] The scanning electron microscopy (SEM) images showed that the PAFs had a uniform spherical particle morphology (Fig. S7†). Energy-dispersive spectrometry (EDS) elemental mapping clearly evidenced that the C, O and S elements were evenly distributed (Fig. 2d). The actual elemental contents of these samples are listed in Table S1.† The thermogravimetric analysis (TGA) of PAFs under the air showed that they have good thermal stability (Fig. S8 and S9†).

Bromophenol blue belongs to a class of dye molecules, which are often used as pH indicators due to their switchable optical absorptivity. The BPB molecules in aqueous solution show different oxidation states under different pH conditions, and the sultone group undergoes reversible "open-loop" and "closed-loop" responses. If PAF materials based on bromophenol blue can retain the reversible structural response as the BPB molecules, after alkali treatment, the material will generate abundant free sulfonic acidic groups that can greatly promote the ion conductive efficiency. Therefore, the synthesized PAF samples were soaked and stirred with 1 mol per L HCl (pH = 0) and 1 mol per L NaOH (pH = 14) solution, respectively, which are denoted as PAF-H (after hydrochloric acidic treatment) and PAF-OH (after sodium hydroxide treatment). The structural changes of the PAF-H and PAF-OH materials were further characterized by UV-vis spectroscopy. In the UV-vis spectrum of the bromophenol blue solution, different pH conditions led to different absorptions and colors. As shown in Fig. 2e, bromophenol blue was orange at pH = 0 with the main absorption peak at 436 nm. At pH = 14, the color of BPB was blue-purple, and the main absorption peak changed to 590 nm. The experimental results are consistent with those reported in the literature.[57,58] The solid UV-vis spectra of PAFs treated with 1 mol per L HCl and NaOH solutions were also tested, respectively. It was found that both PAF-125-OH and PAF-126-OH exhibited

new absorption peaks or a significant enhancement in the peak at 590 nm (Fig. 2f and S10†). The color of the PAF solid powders also changed significantly, indicating that the PAF materials indeed undergo structural changes after 1 mol per L HCl and 1 mol per L NaOH treatment. Furthermore, to elucidate bond formation and transformations within the structure, we conducted ^{13}C solid-state nuclear magnetic resonance (NMR) measurements utilizing the cross-polarization magic-angle spinning (CP/MAS) technique, as illustrated in Fig. 2g. The observed chemical shifts in the range of 105–102 ppm are indicative of sp^3 hybridized carbons originating from BPB and unsaturated carbons from the RC≡CR groups, thereby providing additional evidence for the successful coupling of the monomeric units. It was also observed that the major peaks and chemical shifts of PAF-H and PAF-OH showed no obvious changes, indicating good stability of the material frameworks. The emergence of a new and significant carbon chemical shift near 166 ppm might originate from the C=O of benzoquinone,[59] which is caused by the "open-loop" state of the sultone group after 1 mol per L NaOH treatment. According to the above discussion, the PAF materials constructed from bromophenol blue indicator exhibit reversible structural "open-loop" and "closed-loop" responses because of their sultone group under acidic and alkaline environments, as predicted.

Ion conduction properties

From the structural characterization and adsorption results of PAFs, it can be predicted that a large number of free sulfonic acidic groups are generated by the structural "open-loop" response of the sultone group under alkali conditions, and their good affinity for water molecules may promote the PAFs to exhibit superior ion conductivity. Hence, the ion conductivity performances of PAF-H and PAF-OH were investigated. The impedance Nyquist plots of PAF-126-OH at 25 °C and different humidity conditions were obtained. As shown in Fig. S11,† the resistance value of the PAF-126-OH material decreased with an increase in relative humidity (RH), and ion conductivity at 95% RH reached 1.71×10^{-4} S cm^{-1}, indicating that high relative humidity is conducive to the conduction of ions, which is in agreement with the water vapor adsorption test result. The impedance Nyquist plots of PAF-H and PAF-OH materials at different temperatures and 98% relative humidity were further measured. The results showed that the ion conductivity of PAF-125-OH increased with the increase in temperature, and the ion conductivity at 85 °C and 98% RH was as high as 1.38×10^{-1} S cm^{-1} (Fig. S12†). Similarly, PAF-126-OH showed the same change rule, and the ion conductivity reached 1.4×10^{-1} S cm^{-1} (95 °C, 98% RH) (Fig. 3a). On the contrary, the ion conductivities of PAF-H materials after 1 mol per L HCl treatment showed significant differences, as follows: 3.4×10^{-3} S cm^{-1} (85 °C, 98% RH) for PAF-125-H and 8.89×10^{-3} S cm^{-1} (95 °C, 98% RH) for PAF-126-H (Fig. 3b and S13†). At 25 °C, the ion conductivities (10^{-3}–10^{-2} S cm^{-1}) of the PAF-OH materials were higher by 4 orders of magnitude than those (10^{-7}–10^{-6} S cm^{-1}) of the PAF-H materials. The detailed results of ion conductivity are listed in Table S2.† These changes are mainly attributed to the large number of free sulfonic acidic groups generated by the structural "open-loop" behavior of the sultone group in the PAF-OH material, which greatly promotes the transfer of ions in the channels. To the best of our knowledge, such porous materials with high ion conductivity triggered by acid/base switching have not been reported yet.

To further study the ion conduction mechanism of PAFs, the activation energy (E_a) values were calculated by using the

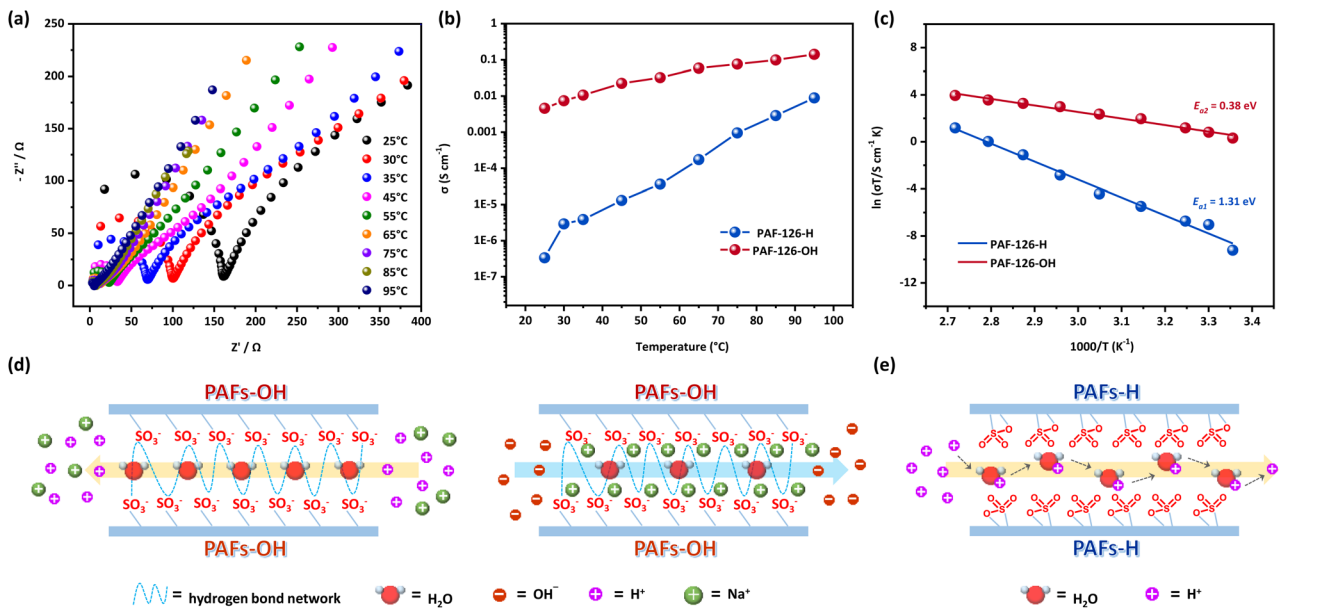

Fig. 3 (a) Nyquist plots of PAF-126-OH at different temperatures under 98% RH. (b) Temperature-dependent ion conductivities of PAF-126-H and PAF-126-OH under 98% RH. (c) Arrhenius plots of PAF-126-H and PAF-126-OH under 98% RH. Illustrations of the possible ion transport mechanism in the PAFs: (d) PAF-126-OH and (e) PAF-126-H.

Arrhenius equation based on the temperature-dependent conductivity profiles. Fig. 3c and S14† display that the activation energies of PAF-125-OH and PAF-126-OH materials were 0.25 eV and 0.38 eV respectively, which can be classified as the conventional Grotthuss mechanism (0.1–0.4 eV, also known as the hopping mechanism).[60–63] In contrast, both PAF-125-H and PAF-126-H materials exhibited much higher activation energies of 0.86 eV and 1.31 eV, respectively. Such high activation energies are more consistent with the vehicle mechanism (>0.5 eV). Hence, the possible ion pathways and transfer mechanisms in PAFs can be further understood by combining with the results of structure analysis, water-vapor adsorption and activation energy calculations. In PAF-OH materials treated with NaOH solution, the large number of free $-SO_3^-$ groups formed easily cooperate with the adsorbed water molecules to build a continuous hydrogen bond network, which serves as the Na^+/H^+ transfer pathway in the channels, as shown in Fig. 3d. Moreover, the residual OH^- anions in the pores after 1 mol per L NaOH treatment can also offer a continuous conduction pathway through Na^+ cations that act as hopping sites. Thus, the cooperative transport of multiple ions in the PAF channels achieves ultrahigh ionic conductivity. However, for PAF-H materials, the sultone configurations formed by the "closed-loop" behavior hinder the formation of a continuous hydrogen bond network and result in high activation energy. Therefore, H^+ can only be transported in the channels through the self-diffusion of water molecules, which serve as carriers (Fig. 3e), conforming to the vehicle mechanism. Considering the high stability of PAFs, the cyclic stability of ion conductivity during acid/base switch response was investigated. Activated PAF materials were selected and treated with 1 mol per L HCl and NaOH solutions 10 times. The ion conductivity of the samples after each treatment was tested at 25 °C under 98% RH. As shown in Fig. S15 and S16,† the obtained results demonstrate that PAFs have excellent and stable ion conductivity with acid/base switchable response.

To demonstrate the practical value of these PAFs, continuous PAF-126 membranes (denoted as PAF-126M) were prepared using the surface-initiated polymerization strategy,[36,43,56,64] as shown in Fig. 4a. Its optical image in Fig. 4b shows that the continuous PAF membrane could be easily detached from the silicon wafer surface and transferred to any other substrate. The size (1 cm × 1 cm) and shape of the continuous membrane depend largely on the original silica substrate. The characteristic vibrations in the IR spectra (Fig. S17†) of the continuous membrane were consistent with the powder material, proving the successful preparation of the material. XPS also proved the existence of the S element (167 eV for S_{2p}), as shown in Fig. S18.† Atomic Force Microscopy (AFM) was further used to measure membrane thickness at several points around its edge, which was 50 nm on average (Fig. 4c). Such nanoscale thickness is highly desirable for ion conductive membranes as it enhances the efficiency of ion transport. Moreover, the SEM and EDS images indicate that the obtained PAF-126M was continuous (Fig. S19 and S20†). The PXRD patterns show that the PAF continuous membrane was amorphous (Fig. S21†). The water contact angle of the PAF continuous membrane was further tested. The result demonstrates that the PAF-126M exhibited excellent hydrophilicity (Fig. S22a†) as the membrane was thin and contained readily exposed hydrophilic groups within the pores. In contrast, the surface of the PAF-126 powder also exhibited certain hydrophobicity (Fig. S22b†). This is consistent with the water adsorption curve, which shows minimal water adsorption in the low-pressure region, indicating the hydrophobic nature of the PAF particle surface. However, when the pressure reaches a certain threshold, water molecules enter the pores, leading to a pronounced hydrophilic behavior.

The membrane was then transferred to an inter-digitated gold electrode and the impedance was measured at different temperature and humidity conditions after soaking in 1 mol per L HCl and 1 mol per L NaOH solutions. The Nyquist plots of PAF-126M-OH (after soaking in 1 mol L^{-1} NaOH solution) and PAF-126M-H (after soaking in 1 mol per L HCl solution) are shown in Fig. 4d and e, respectively. Surprisingly, the ion conductivity of the PAF-126M-OH membrane reached up to 7.29×10^{-1} S cm^{-1} (85 °C, 98% RH), while it remained at 1.5×10^{-1} S cm^{-1} at 30 °C and 98% RH. On the contrary, the ion conductivity of PAF-126M-H was only 3.8×10^{-3} S cm^{-1} (30 °C, 98% RH) (Fig. 4f). The detailed results of ion conductivity are listed in Table S3.†

The activation energies (E_a) (Fig. 4g) of the PAF-126M-OH and PAF-126M-H membranes were calculated to be 0.27 eV and 0.29 eV, respectively, which are all lower than those of the PAF-126-OH (0.38 eV) and PAF-126-H powders (1.31 eV), respectively. It can be understood that in powder samples, the ion transfer process not only requires continuous functional sites within the channels but also needs to overcome the influence of particle stacking voids. In a continuous membrane with nanoscale thickness and structural continuity, particle stacking voids do not influence the ion transfer process, thus requiring smaller activation energy. Furthermore, the ion transfer processes in the PAF-126M-OH and PAF-126M-H membranes conform to the Grotthuss mechanism. For PAF-126M-H, it may be because of the thin and continuous membrane with good uniformity, and ions can also hop *via* the hydrogen bonds between sultone and water molecules, but the transfer efficiency is far lower than that offered by free sulfonic acidic groups. Thus, there is a significant difference in ion conductivity between the membrane materials treated with 1 mol per L HCl and 1 mol per L NaOH solutions. Furthermore, a series of ion conductivity tests were performed on the PAF membrane materials across a range of pH conditions. The results reveal the pronounced sensitivity of PAF-126M to both alkaline and acidic environments. Specifically, PAF-126M exhibited a relatively high ionic conductivity of 10^{-1} S cm^{-1} in the pH range of 8 to 12 at 30 °C, while a significantly lower ionic conductivity of 10^{-3} S cm^{-1} was observed in the pH range of 2 to 5 (Fig. S23†). The stability and cyclic responsiveness of the membrane were also measured. The membrane could maintain high ion conductivity after continuous operation for 30 hours at 85 °C and 98% RH (Fig. 4h), while also exhibiting good acid/base switchable cyclic performance (Fig. 4i). In addition, emerging porous materials with high ion conductivity reported in recent years are summarized in Table S4† and compared with

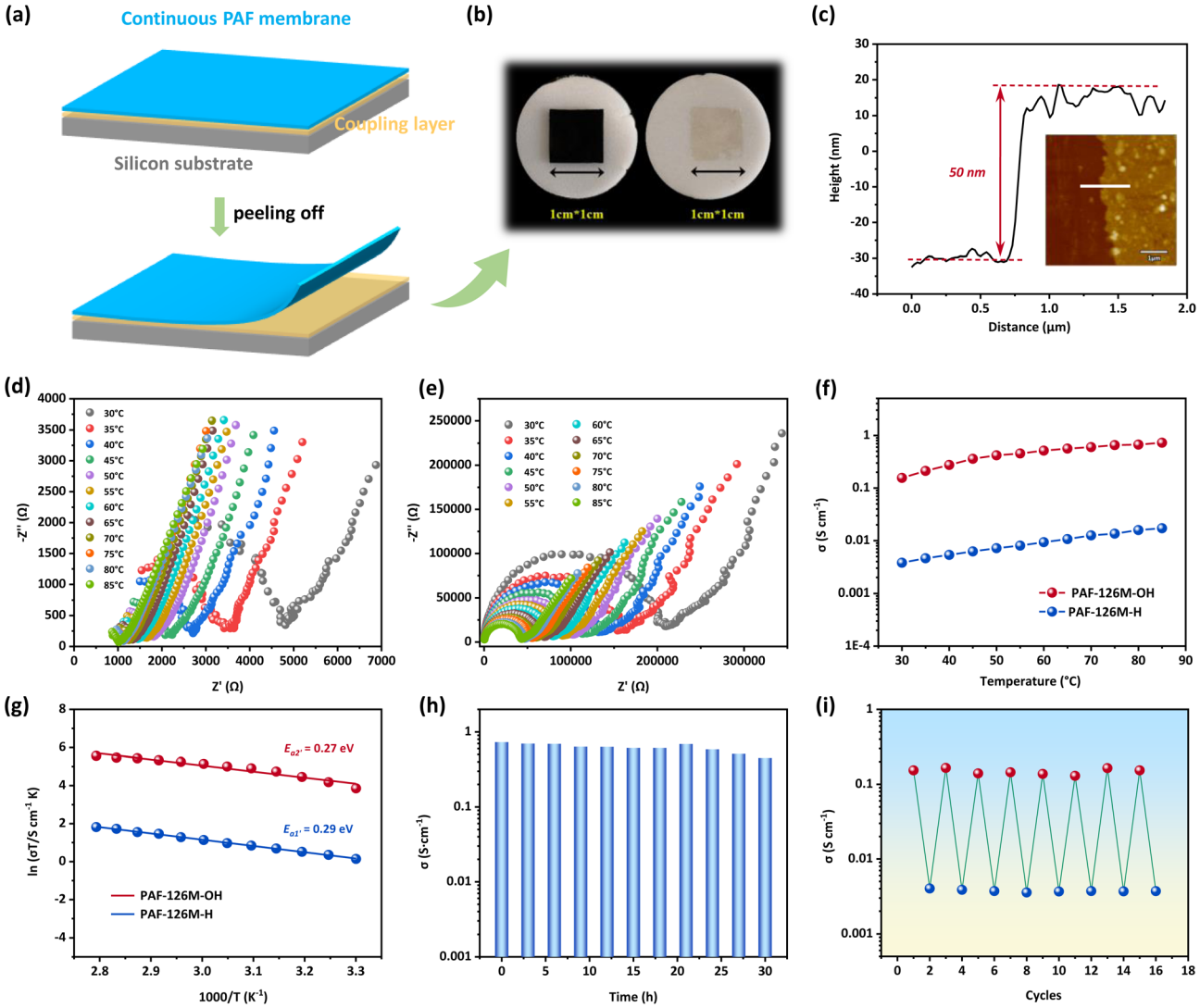

Fig. 4 (a) Preparation of a continuous PAF membrane using the strategy of surface-initiated polymerization. (b) Optical photograph of a continuous PAF-126 membrane detached from a silicon wafer surface. (c) AFM scan and the corresponding section view of the PAF-126 membrane grafted on a silicon substrate. (d) Nyquist plots of PAF-126M-OH at different temperatures under 98% RH. (e) Nyquist plots of PAF-126M-H at different temperatures under 98% RH. (f) Temperature-dependent ion conductivities of PAF-126M-OH and PAF-126M-H under 98% RH. (g) Arrhenius plots of PAF-126M-OH and PAF-126M-H under 98% RH. (h) Time-dependent ion conductivities of PAF-126M-OH performed at 85 °C and 98% RH. (i) Reversible ion conductivity of the continuous PAF-126 membrane after soaking in 1 mol per L NaOH and 1 mol per L HCl solutions at 30 °C and 98% RH.

the PAF continuous membrane synthesized in this work. The ion conductivity of the PAF membrane have exceeded those reported for most of the porous materials. With such high ion conductivity and the ability to be triggered by external acid/base chemical stimuli, the continuous PAF membrane shows great potential to be used as an ion conductor in advanced devices in the future.

Conclusions

In summary, acid/base responsive PAF powders and continuous membranes have been successfully constructed in this work by using a commercially available pH indicator as the functional building unit. The PAFs exhibit the same characteristics of reversible structural responses as the bromophenol blue indicator molecules in acidic and alkali environments. At 25 °C and 98% RH, the ion conductivities of PAF powder reveal an interesting switch of up to 4 orders of magnitude from 3.36×10^{-7} S cm^{-1} after 1 mol per L HCl treatment to 4.59×10^{-3} S cm^{-1} after 1 mol per L NaOH treatment. The main reason for this behavior is that the free sulfonic acidic groups form a continuous hydrogen bonding network with water molecules after treatment with 1 mol per L NaOH, greatly promoting ion hopping transport. At 85 °C and 98% RH, the continuous PAF membrane exhibits ultrahigh ion conductivity of 7.29×10^{-1} S cm^{-1}. Meanwhile, benefiting from the ultrastability of PAFs, the continuous membrane also shows good ion conduction stability and acid/base switchable cyclic performance. This

novel report on ion-conducting membranes with dynamic response to chemical acid/base stimuli may further open up opportunities for the development of innovative ion-conducting materials for application in smart devices and alkaline fuel cells.

Data availability

The data supporting this article have been included as part of the ESI.†

Author contributions

Jian Song and Hengtao Lei contributed equally to this work. Guangshan Zhu and Yuyang Tian conceived and supervised the project. Jian Song and Hengtao Lei designed and carried out the experiments, analyzed the data, and wrote the manuscript. Lin Lin, Mengxiao Sun, Xueyan Han, and Zilong Dou participated in material synthesis and characterization. All authors discussed the results and commented on the manuscript.

Conflicts of interest

There are no conflicts to declare.

Acknowledgements

This work was supported by the Jilin Provincial Scientific and Technological Development Program (20240602105RC), China Postdoctoral Science Foundation (2024T170120, 2023M740577), National Natural Science Foundation of China (22131004, U21A20330, 22075040), the "111" Project (B18012), Fundamental Research Funds for the Central Universities (2412023QD013), and Postdoctoral Funding Project of Jilin Province, China.

References

1 Z. Chen and Y. Zheng, Persistent and responsive collective motion with adaptive time delay, *Sci. Adv.*, 2024, **10**, eadk3914.
2 X. Qian, Y. Zhao, Y. Alsaid, X. Wang, M. Hua, T. Galy, H. Gopalakrishna, Y. Yang, J. Cui, N. Liu, M. Marszewski, L. Pilon, H. Jiang and X. He, Artificial phototropism for omnidirectional tracking and harvesting of light, *Nat. Nanotechnol.*, 2019, **14**, 1048–1055.
3 S. Wang and M. W. Urban, Redefining polymer science *via* multi-stimulus responsiveness, *Chem*, 2023, **9**, 1362–1377.
4 E. Benchimol, J. Tessarolo and G. H. Clever, Photoswitchable coordination cages, *Nat. Chem.*, 2024, **16**, 13–21.
5 H. Qin, T. Zhang, N. Li, H.-P. Cong and S.-H. Yu, Anisotropic and self-healing hydrogels with multi-responsive actuating capability, *Nat. Commun.*, 2019, **10**, 2202.
6 P. She, Y. Qin, X. Wang and Q. Zhang, Recent Progress in External-Stimulus-Responsive 2D Covalent Organic Frameworks, *Adv. Mater.*, 2022, **34**, 2101175.
7 W. Wei, L. He, G. Han, Y. Lu, S. Shi, Z. Yuan, X. Wang, Y. Li, B. Chen, Z. Zhang and S. Xiang, Stimulus-responsive hydrogen-bonded organic frameworks: construction strategies, research progress and applications, *Coord. Chem. Rev.*, 2024, **507**, 215760.
8 P. Liu, F. Fang, H. Wang and N. M. Khashab, Smart Materials Based on Synthetic Host Molecules: The Role of Host–Guest Chemistry in the Fabrication and Application, *Angew. Chem., Int. Ed.*, 2023, **62**, e202218706.
9 W. Ji, J. Liang, J. Zhou, H. Huang, D. Qu, S. Pang and X. Ai, Built-in stimuli-responsive designs for safe and reliable electrochemical energy storage devices—a review, *Energy Storage Mater.*, 2023, **63**, 102945.
10 Y. Su, K.-i. Otake, J.-J. Zheng, H. Xu, Q. Wang, H. Liu, F. Huang, P. Wang, S. Kitagawa and C. Gu, Switching molecular recognition selectivities by temperature in a diffusion-regulatory porous material, *Nat. Commun.*, 2024, **15**, 144.
11 R. D. Jansen-van Vuuren, S. Naficy, M. Ramezani, M. Cunningham and P. Jessop, CO_2-responsive gels, *Chem. Soc. Rev.*, 2023, **52**, 3470–3542.
12 X. Li, M. Shen, J. Yang, L. Liu and Y.-W. Yang, Pillararene-Based Stimuli-Responsive Supramolecular Delivery Systems for Cancer Therapy, *Adv. Mater.*, 2024, **36**, 2313317.
13 N. Asadi-Zaki, H. Mardani, H. Roghani-Mamaqani and F. Wang, Stimuli-induced adjustment of spatial distribution of fluorescence resonance energy transfer dyads in smart polymers, *Coord. Chem. Rev.*, 2024, **500**, 215518.
14 Y. Shen, X. Le, Y. Wu and T. Chen, Stimulus-responsive polymer materials toward multi-mode and multi-level information anti-counterfeiting: recent advances and future challenges, *Chem. Soc. Rev.*, 2024, **53**, 606–623.
15 W. Feng, Q. He and L. Zhang, Embedded Physical Intelligence in Liquid Crystalline Polymer Actuators and Robots, *Adv. Mater.*, 2024, 2312313, DOI: **10.1002/adma.202312313**.
16 T. Yimyai, D. Crespy and M. Rohwerder, Corrosion-Responsive Self-Healing Coatings, *Adv. Mater.*, 2023, **35**, 2300101.
17 M. Lago-Silva, M. Fernández-Míguez, R. Rodríguez, E. Quiñoá and F. Freire, Stimuli-responsive synthetic helical polymers, *Chem. Soc. Rev.*, 2024, **53**, 793–852.
18 M. Bayat, H. Mardani, H. Roghani-Mamaqani and R. Hoogenboom, Self-indicating polymers: a pathway to intelligent materials, *Chem. Soc. Rev.*, 2024, **53**, 4045–4085.
19 Y. Wu, D. Wang, I. Willner, Y. Tian and L. Jiang, Smart DNA Hydrogel Integrated Nanochannels with High Ion Flux and Adjustable Selective Ionic Transport, *Angew. Chem., Int. Ed.*, 2018, **57**, 7790–7794.
20 M. Ahmad, S. A. Gartland and M. J. Langton, Photo- and Redox-Regulated Transmembrane Ion Transporters, *Angew. Chem., Int. Ed.*, 2023, **62**, e202308842.
21 J. de Jong, J. E. Bos and S. J. Wezenberg, Stimulus-Controlled Anion Binding and Transport by Synthetic Receptors, *Chem. Rev.*, 2023, **123**, 8530–8574.

22 X. Zhang, L. Xie, S. Zhou, H. Zeng, J. Zeng, T. Liu, Q. Liang, M. Yan, Y. He, K. Liang, L. Zhang, P. Chen, L. Jiang and B. Kong, Interfacial Superassembly of Mesoporous Titania Nanopillar-Arrays/Alumina Oxide Heterochannels for Light- and pH-Responsive Smart Ion Transport, *ACS Cent. Sci.*, 2022, **8**, 361–369.

23 K. Xiao, G. Xie, P. Li, Q. Liu, G. Hou, Z. Zhang, J. Ma, Y. Tian, L. Wen and L. Jiang, A Biomimetic Multi-Stimuli-Response Ionic Gate Using a Hydroxypyrene Derivation-Functionalized Asymmetric Single Nanochannel, *Adv. Mater.*, 2014, **26**, 6560–6565.

24 F. Xiang, S. Chen, Z. Yuan, L. Li, Z. Fan, Z. Yao, C. Liu, S. Xiang and Z. Zhang, Switched Proton Conduction in Metal–Organic Frameworks, *JACS Au*, 2022, **2**, 1043–1053.

25 H.-Q. Liang, Y. Guo, Y. Shi, X. Peng, B. Liang and B. Chen, A Light-Responsive Metal–Organic Framework Hybrid Membrane with High On/Off Photoswitchable Proton Conductivity, *Angew. Chem., Int. Ed.*, 2020, **59**, 7732–7737.

26 K. Müller, J. Helfferich, F. Zhao, R. Verma, A. B. Kanj, V. Meded, D. Bléger, W. Wenzel and L. Heinke, Switching the Proton Conduction in Nanoporous, Crystalline Materials by Light, *Adv. Mater.*, 2018, **30**, 1706551.

27 S. S. Nagarkar, S. Horike, T. Itakura, B. Le Ouay, A. Demessence, M. Tsujimoto and S. Kitagawa, Enhanced and Optically Switchable Proton Conductivity in a Melting Coordination Polymer Crystal, *Angew. Chem., Int. Ed.*, 2017, **56**, 4976–4981.

28 T. Ben, H. Ren, S. Ma, D. Cao, J. Lan, X. Jing, W. Wang, J. Xu, F. Deng, J. M. Simmons, S. Qiu and G. Zhu, Targeted Synthesis of a Porous Aromatic Framework with High Stability and Exceptionally High Surface Area, *Angew. Chem., Int. Ed.*, 2009, **48**, 9457–9460.

29 Y. Tian and G. Zhu, Porous Aromatic Frameworks (PAFs), *Chem. Rev.*, 2020, **120**, 8934–8986.

30 Y. Yuan and G. Zhu, Porous Aromatic Frameworks as a Platform for Multifunctional Applications, *ACS Cent. Sci.*, 2019, **5**, 409–418.

31 A. A. Uliana, N. T. Bui, J. Kamcev, M. K. Taylor, J. J. Urban and J. R. Long, Ion-capture electrodialysis using multifunctional adsorptive membranes, *Science*, 2021, **372**, 296–299.

32 B. Li, Y. Zhang, R. Krishna, K. Yao, Y. Han, Z. Wu, D. Ma, Z. Shi, T. Pham, B. Space, J. Liu, P. K. Thallapally, J. Liu, M. Chrzanowski and S. Ma, Introduction of π-Complexation into Porous Aromatic Framework for Highly Selective Adsorption of Ethylene over Ethane, *J. Am. Chem. Soc.*, 2014, **136**, 8654–8660.

33 Z. Wang, Q. Meng, R. Ma, Z. Wang, Y. Yang, H. Sha, X. Ma, X. Ruan, X. Zou, Y. Yuan and G. Zhu, Constructing an Ion Pathway for Uranium Extraction from Seawater, *Chem*, 2020, **6**, 1683–1691.

34 J. Kamcev, M. K. Taylor, D.-M. Shin, N. N. Jarenwattananon, K. A. Colwell and J. R. Long, Functionalized Porous Aromatic Frameworks as High-Performance Adsorbents for the Rapid Removal of Boric Acid from Water, *Adv. Mater.*, 2019, **31**, 1808027.

35 Y. Yuan, F. Sun, L. Li, P. Cui and G. Zhu, Porous aromatic frameworks with anion-templated pore apertures serving as polymeric sieves, *Nat. Commun.*, 2014, **5**, 4260.

36 Y. Ma, F. Cui, H. Rong, J. Song, X. Jing, Y. Tian and G. Zhu, Continuous Porous Aromatic Framework Membranes with Modifiable Sites for Optimized Gas Separation, *Angew. Chem., Int. Ed.*, 2022, **61**, e202113682.

37 M. Ratsch, C. Ye, Y. Yang, A. Zhang, A. M. Evans and K. Börjesson, All-Carbon-Linked Continuous Three-Dimensional Porous Aromatic Framework Films with Nanometer-Precise Controllable Thickness, *J. Am. Chem. Soc.*, 2020, **142**, 6548–6553.

38 J. Song, Y. Li, P. Cao, X. Jing, M. Faheem, Y. Matsuo, Y. Zhu, Y. Tian, X. Wang and G. Zhu, Synergic Catalysts of Polyoxometalate@Cationic Porous Aromatic Frameworks: Reciprocal Modulation of Both Capture and Conversion Materials, *Adv. Mater.*, 2019, **31**, 1902444.

39 L. Cao, C. Wang, H. Wang, X. Xu, X. Tao, H. Tan and G. Zhu, Rationally Designed Cyclooctatetrathiophene-Based Porous Aromatic Frameworks (COTh-PAFs) for Efficient Photocatalytic Hydrogen Peroxide Production, *Angew. Chem., Int. Ed.*, 2024, **63**, e202402095.

40 S. Lee, G. Barin, C. M. Ackerman, A. Muchenditsi, J. Xu, J. A. Reimer, S. Lutsenko, J. R. Long and C. J. Chang, Copper Capture in a Thioether-Functionalized Porous Polymer Applied to the Detection of Wilson's Disease, *J. Am. Chem. Soc.*, 2016, **138**, 7603–7609.

41 J. Wang, X. Zhang, Z. Liu, J. Yu, H.-G. Wang, X.-L. Wu, F. Cui and G. Zhu, Tuning Electron Delocalization of Redox-Active Porous Aromatic Framework for Low-Temperature Aqueous Zn–K Hybrid Batteries with Air Self-Chargeability, *Angew. Chem., Int. Ed.*, 2024, **63**, e202401559.

42 J. Zou, A. Trewin, T. Ben and S. Qiu, High Uptake and Fast Transportation of LiPF6 in a Porous Aromatic Framework for Solid-State Li-Ion Batteries, *Angew. Chem., Int. Ed.*, 2020, **59**, 769–774.

43 W. Du, L. Liu, L. Yin, B. Li, Y. Ma, X. Guo, H.-Y. Zang, N. Zhang and G. Zhu, Ultrathin Free-Standing Porous Aromatic Framework Membranes for Efficient Anion Transport, *Angew. Chem., Int. Ed.*, 2024, **63**, e202402943.

44 Y. Ye, L. Gong, S. Xiang, Z. Zhang and B. Chen, Metal–Organic Frameworks as a Versatile Platform for Proton Conductors, *Adv. Mater.*, 2020, **32**, 1907090.

45 Z. Guo, Y. Zhang, Y. Dong, J. Li, S. Li, P. Shao, X. Feng and B. Wang, Fast Ion Transport Pathway Provided by Polyethylene Glycol Confined in Covalent Organic Frameworks, *J. Am. Chem. Soc.*, 2019, **141**, 1923–1927.

46 H.-Y. Li, C. Li, Y.-Y. Wang, W.-D. Dong, X.-K. Zhang, M.-H. Sun, Y. Li and B.-L. Su, Pore structure unveiling effect to boost lithium–selenium batteries: selenium confined in hierarchically porous carbon derived from aluminum based MOFs, *Chem. Synth.*, 2023, **3**, 30.

47 H.-Y. Li, C. Li, Y.-Y. Wang, M.-H. Sun, W. Dong, Y. Li and B.-L. Su, Selenium confined in ZIF-8 derived porous carbon@MWCNTs 3D networks: tailoring reaction kinetics for high performance lithium–selenium batteries, *Chem. Synth.*, 2022, **2**, 8.

48 H. Li, R. Meng, C. Ye, A. Tadich, W. Hua, Q. Gu, B. Johannessen, X. Chen, K. Davey and S.-Z. Qiao, Developing high-power Li‖S batteries *via* transition metal/carbon nanocomposite electrocatalyst engineering, *Nat. Nanotechnol.*, 2024, **19**, 792.

49 H. Wu, J. Hao, Y. Jiang, Y. Jiao, J. Liu, X. Xu, K. Davey, C. Wang and S.-Z. Qiao, Alkaline-based aqueous sodium-ion batteries for large-scale energy storage, *Nat. Commun.*, 2024, **15**, 575.

50 Z. Chen, P. Fang, J. Li, X. Han, W. Huang, W. Cui, Z. Liu, M. R Warren, D. Allan, P. Cheng, S. Yang and W. Shi, Rapid extraction of trace benzene by a crown-ether-based metal–organic framework, *Natl. Sci. Rev.*, 2024, **11**, nwae342.

51 J. Liu, J. Jiang, Q. Zhou, Z. Chen, R. Zhang, X. Xu, X. Han, S. Yang, Z. Zhou, P. Cheng and W. Shi, Manipulation of π-aromatic conjugation in two-dimensional Sn-organic materials for efficient lithium storage, *eScience*, 2023, **3**, 100094.

52 S. Qiu, M. Xue and G. Zhu, Metal–organic framework membranes: from synthesis to separation application, *Chem. Soc. Rev.*, 2014, **43**, 6116–6140.

53 Y. Cheng, S. J. Datta, S. Zhou, J. Jia, O. Shekhah and M. Eddaoudi, Advances in metal–organic framework-based membranes, *Chem. Soc. Rev.*, 2022, **51**, 8300–8350.

54 S. Yuan, X. Li, J. Zhu, G. Zhang, P. Van Puyvelde and B. Van der Bruggen, Covalent organic frameworks for membrane separation, *Chem. Soc. Rev.*, 2019, **48**, 2665–2681.

55 W. J. Phang, H. Jo, W. R. Lee, J. H. Song, K. Yoo, B. Kim and C. S. Hong, Superprotonic Conductivity of a UiO-66 Framework Functionalized with Sulfonic Acid Groups by Facile Postsynthetic Oxidation, *Angew. Chem., Int. Ed.*, 2015, **54**, 5142–5146.

56 L. Liu, L. Yin, D. Cheng, S. Zhao, H.-Y. Zang, N. Zhang and G. Zhu, Surface-Mediated Construction of an Ultrathin Free-Standing Covalent Organic Framework Membrane for Efficient Proton Conduction, *Angew. Chem., Int. Ed.*, 2021, **60**, 14875–14880.

57 A. Saydjari, J. J. Pietron and B. S. Simpkins, Electrochemical Deposition and Spectroelectrochemical Response of Bromophenol Blue Films on Gold, *Electroanalysis*, 2015, **27**, 1960–1967.

58 J. Ferreira and E. M. Girotto, Optical pH sensitive material based on bromophenol blue-doped polypyrrole, *Sens. Actuators, B*, 2009, **137**, 426–431.

59 R. Shi, L. Liu, Y. Lu, C. Wang, Y. Li, L. Li, Z. Yan and J. Chen, Nitrogen-rich covalent organic frameworks with multiple carbonyls for high-performance sodium batteries, *Nat. Commun.*, 2020, **11**, 178.

60 H. Xu, S. Tao and D. Jiang, Proton conduction in crystalline and porous covalent organic frameworks, *Nat. Mater.*, 2016, **15**, 722–726.

61 H. S. Sasmal, H. B. Aiyappa, S. N. Bhange, S. Karak, A. Halder, S. Kurungot and R. Banerjee, Superprotonic Conductivity in Flexible Porous Covalent Organic Framework Membranes, *Angew. Chem., Int. Ed.*, 2018, **57**, 10894–10898.

62 F.-M. Zhang, L.-Z. Dong, J.-S. Qin, W. Guan, J. Liu, S.-L. Li, M. Lu, Y.-Q. Lan, Z.-M. Su and H.-C. Zhou, Effect of Imidazole Arrangements on Proton-Conductivity in Metal–Organic Frameworks, *J. Am. Chem. Soc.*, 2017, **139**, 6183–6189.

63 F. Yang, G. Xu, Y. Dou, B. Wang, H. Zhang, H. Wu, W. Zhou, J.-R. Li and B. Chen, A flexible metal–organic framework with a high density of sulfonic acid sites for proton conduction, *Nat. Energy*, 2017, **2**, 877–883.

64 B. Liang, H. Wang, X. Shi, B. Shen, X. He, Z. A. Ghazi, N. A. Khan, H. Sin, A. M. Khattak, L. Li and Z. Tang, Microporous membranes comprising conjugated polymers with rigid backbones enable ultrafast organic-solvent nanofiltration, *Nat. Chem.*, 2018, **10**, 961–967.